IEEE Access
Multidisciplinary | Rapid Review | Open Access Journal

Received June 4, 2021, accepted June 21, 2021, date of publication July 1, 2021, date of current version July 14, 2021.

Digital Object Identifier 10.1109/ACCESS.2021.3093898

Investigation on Rotated Rectangular Slots to Improve the Circular Polarization in Cylindrical Dielectric Resonator Antenna

REENA KUMARI[1,2], RAVI KUMAR GANGWAR[2], (Senior Member, IEEE), AND RAGHVENDRA KUMAR CHAUDHARY[2], (Senior Member, IEEE)

[1]Department of Electronics and Communication Engineering, Vignan's Foundation for Science, Technology and Research (VFSTR), Vadlamudi, Andhra Pradesh 522213, India
[2]Department of Electronics Engineering, Indian Institute of Technology (Indian School of Mines), Dhanbad, Jharkhand 826004, India

Corresponding author: Reena Kumari (reena.31.dec@gmail.com)

This work was supported by the Science and Engineering Research Board (SERB), Department of Science and Technology (DST), India, under Project YSS/2014/000841.

ABSTRACT To achieve wideband circular polarization (CP) characteristics, a new structure with a single feeding technique has been proposed. In the proposed CP structure, to excite the cylindrical dielectric resonator (CDR) four asymmetrical rectangular slots are etched on the ground plane, each rectangular slot is rotated by an angle of ($\theta = 30°$) with respect to its adjacent slots. The electric fields at each slot are separated by 30° in space with respect to its adjacent slot to create 90° angular separations between the E-field components. Two orthogonal broadside modes ($HE_{11\delta}$) are excited inside the cylindrical dielectric resonator antenna (CDRA) independently to obtained CP characteristics. To compare the simulated outcomes with the experimental results, fabrication of the proposed antenna prototype has been done. The measured percentage of bandwidth achieved by the proposed radiator for $|S_{11}|$ and CP is 26.73% and 23.59%, respectively, and the whole usable axial ratio (AR) frequency bands overlap the impedance passband of the presented CP structure. The proposed radiator has achieved the maximum gain and radiation efficiency of 3.4 dB and 95% over the operating frequency range of the designed antenna, respectively. The proposed CP DRA has been configured for the WLAN band application.

INDEX TERMS Axial ratio, circular polarization, dielectric resonator antenna, wideband.

I. INTRODUCTION

The inherent properties offered by dielectric resonator antenna (DRA) is found an appropriate selection for antenna designers due to its high radiation efficiency, small size, lightweight, wideband, and easily excited with various feeding mechanisms [1], [2]. Circularly polarized (CP) DRAs overcome the limitations of linearly polarized (LP) DRAs due to their remarkable features such as the CP systems are insensitive to the problems of antenna misalignment and propagation effects, suppress multipath fading effect, and better mobility in any weather condition [1]–[5]. Due to all these properties, CP DRAs are broadly applicable for satellite applications, mobile communications, navigation systems, and radar [5], [6]. Several feeding mechanisms are presented in the literature for CP operation in DRAs they are single-fed [6], dual or multi-point fed [7]–[9] and sequential rotation feeding technique [10], [11]. The major difficulties found in designing the CP DRAs are maintaining the entire AR passband over the required impedance passband. Therefore, very few designs are available in the literature which has the axial ratio (AR) bandwidth completely covered by its impedance bandwidth. Some designs are reported in the literature such as cross-slot fed square DRA with an overlapping axial ratio bandwidth of 46.9% [12] and a square DRA excited by dual feeding configuration with an overlapping AR bandwidth of 43.5% [13] but due to dual feeding and large antenna dimensions, both structures become complex and bulky, respectively. A square DRA excited by a cross-slot was also stated with an overlapping AR bandwidth

The associate editor coordinating the review of this manuscript and approving it for publication was Davide Ramaccia.

of 22.8% [14]. To generate CP wave by modifying the DR shape or geometry has also been carried out in the reported literature and they are a bow-tie shape DR [6] and cylindrical ring DRA [15]. Therefore, it is a very well-known fact that the ceramic material is very hard in nature due to that it is very difficult to modify its shapes or geometry. Another drawback, it costs more for any special DR geometry or shapes and not easily available in the commercial market. All these modified shape structures [6], [15] are very complex as well as bulky.

In the present article, an innovative technique has been proposed for generating the CP wave by exciting the cylindrical DR with an asymmetrical bow-tie shape slot along with an off-centered microstrip feed without any modification in DR geometry or shape. These observations illustrate that the CP performance can be enhanced by single-point-fed regular-shaped DRAs by utilizing a proper feeding structure. In the proposed configuration, the total AR passband is completely covered by its impedance passband with wideband CP performance. The complete AR frequency band is usable, which is another advantage. In TABLE-1 performance comparison of the proposed antenna with some reported design has shown. So many wideband CP DRAs [12]–[15] are reported in the literature with complete overlapping between impedance and AR bandwidth but they are using complex DR geometry or shapes, multi-point feeding and large antenna dimensions due to that structures become very bulky and complex as compared to the proposed antenna.

TABLE 1. Performance comparison of the proposed antenna.

Shape	f (GHz)	Dimension (mm)	Feeding	S_{11} (% & GHz)	AR (% & GHz)
Ring Cylindrical DRA [15]	26	13.2×13.2×1.524	Cross-slot substrate integrated	33.5 & (20.1-28.5)	26.3 & (20.3-26.45)
Square DRA [12]	2.3/3.4	76×76×19.8	Cross-slot	46.9 (2.19-3.53)	49.5 & (2.19-3.63)
Square DRA [13]	1.9/2.3/2.7	70×70×40	Dual Feeding	55.31 & (1.7 - 3)	43.5 & (1.83 - 2.85)
Square DRA [14]	5/5.5	55×8.828	Cross-slot	25.4 & (4.8-6.2)	22.8 & (4.85-6.1)
Cylindrical DRA [Proposed]	5.5/6/6.5	46×46×10.1	Asymmetrical bow-tie shaped slot	26.73 & (5.25-6.87)	23.59 & (5.42-6.87)

II. ANTENNA GEOMETRY

A slot is etched in the ground plane and the complete slot is a combination of four asymmetrical rectangular-shaped slots. A rotation angle of ($\theta = 30°$) is used to rotate each rectangular slot with respect to its contiguous slots. Since each slot has a 30° rotation with respect to its contiguous slots, therefore, a total angular separation of 90° is created by the four rotated rectangular slots. The geometrical form of the reported CP DRA is illustrated in Fig. 1. The presented design primarily comprises a cylindrical dielectric resonator (DR), a slot that is etched in the ground plane and a microstrip line. The relative permittivity of ($\varepsilon_r = 9.8$, $\tan\delta = 0.002$) is used as a cylindrical DR of radius 'R' and height 'H'. The FR4 epoxy of a dielectric constant ($\varepsilon_{rs} = 4.4$ & $\tan\delta = 0.02$) and dimension ($L_s$mm × W_s mm × t mm) is selected for the substrate. An off-centered 50 Ω microstrip line of length 'L' and width 'W' has been printed on the bottom layer of the substrate. The microstrip line is placed at a distance 'D' with respect to the center position of the substrate in the y-axis direction. With the help of the adhesive material, the cylindrical DR is positioned over the slot. The HFSS simulation software has been utilized to design and optimized the proposed CP radiator.

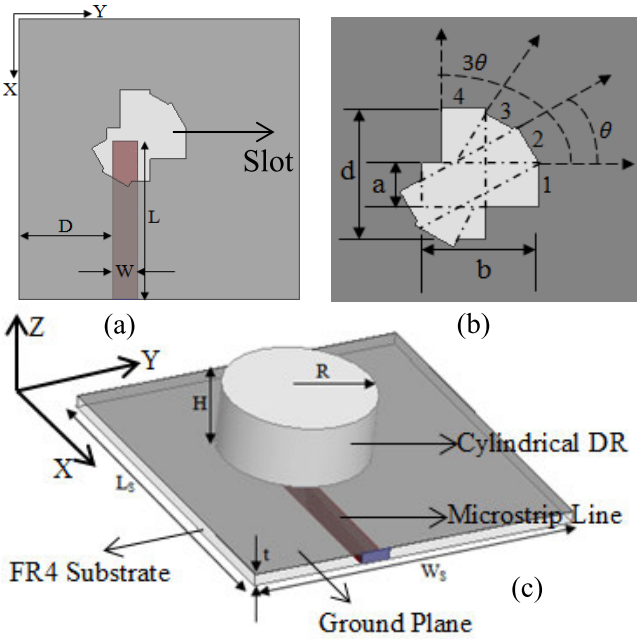

FIGURE 1. Geometrical representation of the designed antenna (a) Feeding Network (b) Slot Geometry (c) Side View. [L_S = 46 mm, W_S = 46 mm, t = 1.6 mm, R = 10 mm, H = 8.5 mm, L = 26 mm, W = 4 mm, D = 15.5 mm, a = 5mm, b = 13 mm, d = 15 mm].

III. ANTENNA ANALYSIS

A. EVOLUTION OF THE PROPOSED ANTENNA DESIGN

The present section deals with the evolution and theoretical background of the presented antenna design in two different approaches for CP generation, which are as follows.

Case I (Horizontal Slot to Vertical Slot): Fig. 2 describes the design procedure of the presented antenna in four different steps. Firstly, a cylindrical DR is fed by a horizontally placed rectangular slot '*1*' of dimension (a mm × b mm) referred to as Antenna 'W' shown in Fig. 2(a). On the next stage as shown in Fig. 2(b), along the azimuthal direction one another rectangular slot '*2*' of dimension (a mm × d mm) is introduced which is displaced by ($\theta = 30°$) in space

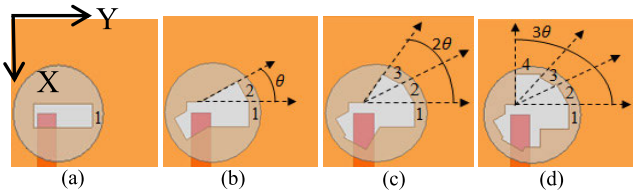

FIGURE 2. Geometrical configuration of the proposed antenna design in four different steps from the horizontal slot to vertical slot direction (a) Antenna 'W' (b) Antenna 'X' (c) Antenna 'Y' (c) Antenna 'Z' (Proposed design).

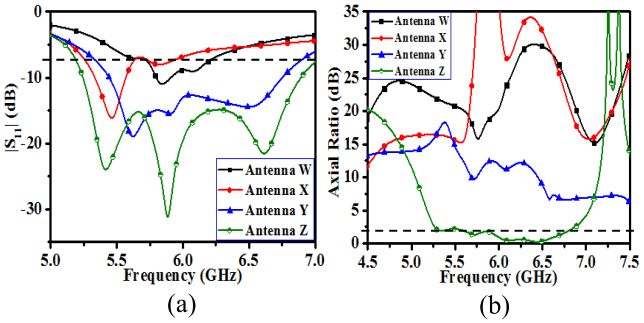

FIGURE 3. (a) Input reflection coefficient and (b) AR of the proposed antenna design in four different steps from the horizontal slot to vertical slot direction.

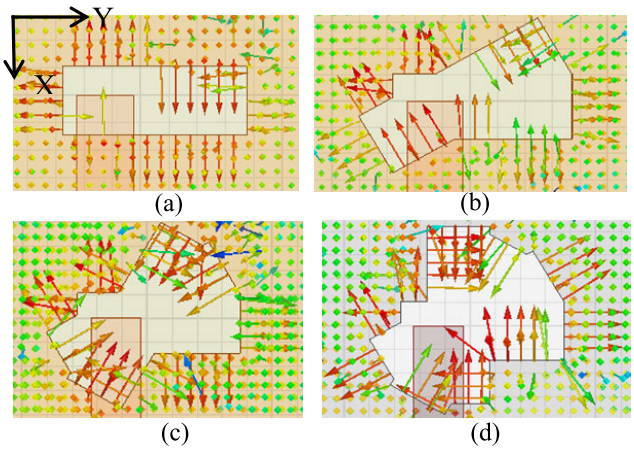

FIGURE 4. E-field distribution during different rotation of asymmetrical rectangular slots from the horizontal slot to vertical slot direction (a) Antenna 'W' at 5.84 GHz (b) Antenna 'X' at 5.45 GHz (c) Antenna 'Y' at 5.6 GHz (c) Antenna 'Z' at 5.4 GHz (Proposed design).

with respect to the slot '*1*' in the counterclockwise direction named as Antenna 'X'. Due to that, ($\boldsymbol{\theta} = 30°$) angular separation is formed between the excited electric fields at slot '*2*' and slot '*1*' in space [16]. As shown in Fig. 2(c), following the similar design process, by introducing rectangular slot '*3*' of the same dimension as slot '*2*' and it is separated by ($\boldsymbol{2\theta} = 60°$) rotation angle in space with respect to the slot '*1*', Antenna 'Y' is formed. Due to that, again ($\boldsymbol{\theta} = 30°$) angular separation is formed between the excited electric fields at slot '*3*' and slot '*2*' in space. In this way, through slot geometry modification, the direction of exciting electric fields have been decomposed inside the rotated slots [16]. Lastly, the proposed antenna 'Z' is designed by introducing rectangular slot '*4*' of similar dimension as slot '*2*' which is displaced by ($3\boldsymbol{\theta} = 90°$) with respect to slot '1' which is shown in Fig. 2(d). Therefore, electric field separation between slot '*4*' and slot '*3*' is 30° in space, between slot '*4*' and slot '*2*', it is 60° in space and electric field at slot '*1*' is separated in space by 90° from electric fields at slot '*4*'. It has been observed that an angular separation of 90° has been created between the electric field components at slot '*1*' and slot '*4*' in space due to the rotation of the different rectangular slots. In Fig. 3(a) and Fig. 3(b), four stages of different antenna configurations $|S_{11}|$ response and AR characteristics have shown respectively. It is important to note here that the non-orthogonal components of the electric field between contiguous slots such as slot '*1*' and slot '*2*', or slot '*2*' and slot '*3*' and slot '*3*' and slot '*4*' also interfere with the far-field and thus worsens the CP bandwidth due to that in case of antenna structures (W, X and Y) no CP wave is excited which is shown in Fig. 3(b) [16]. So, the exciting electric fields have been disturbed by slot geometry modification along the counterclockwise direction and transformed into orthogonal field components (where, the angular separation between slot '*1*' and slot '*4*' is 90°) in the final antenna stage [16]. In Fig. 4, E-fields are plotted at 5.84, 5.45, 5.6 and 5.4 GHz for antenna W, X, Y and Z, respectively, to check the decomposition with its top view of the rotating slots. It has been observed that the $|S_{11}|$ bandwidth is increasing in every forward stage and the axial ratio minimum point is also enhanced from antenna 'W' to 'Z'. This is because with every forward stage, one rotated rectangular slot is embedded in the forward slot geometry due to that ground plane could be explored more modes that are suppressed by it. By introducing the more rotated slots, the hybrid structures excite the more resonating frequencies which are suppressed by the ground plane. In the final stage, a wide impedance and AR bandwidth of 27.01 % and 27.44 % are achieved by the proposed structure 'Z', respectively.

Case II (Vertical Slot to Horizontal Slot): This approach is shown in Fig. 5 in four different steps and their respective $|S_{11}|$ and AR bandwidth curves are also shown in Fig. 6.

In case II the concept of circular polarization mechanism is similar to the case I and it is already discussed in the previous section. Here, in this modification process, only the difference encountered is in every forward stage, the slot is displaced in space with respect to its adjacent slot in clockwise direction started from the vertically placed rectangular slot. When the different rectangular slots are rotated differently along the azimuthal direction like a spiral pattern, the different components of electric fields such as Eslot-1, Eslot-2, Eslot-3 and Eslot-4 are existing within the rotated slots due to the decomposition of the primary E-field. Therefore, different E-field components are separated with different angles in space due to the modification of slot geometry. This analysis is shown in Fig. 7 and Fig. 8, by plotting the E-field inside the rotated slots where each electric field component covers the different path lengths within the rotating

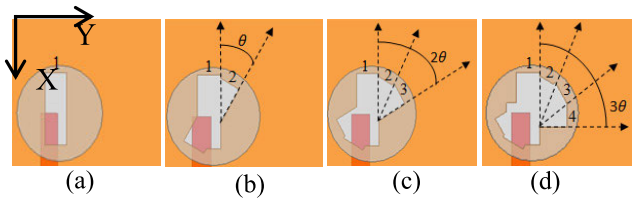

FIGURE 5. Geometrical configuration of the proposed antenna design in four different steps from the vertical slot to horizontal slot direction (a) Antenna 'P' (b) Antenna 'Q' (c) Antenna 'R' (c) Antenna 'S' (Proposed design).

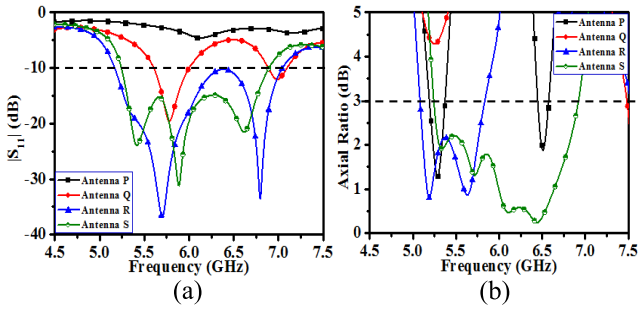

FIGURE 6. (a) $|S_{11}|$ and (b) AR for different antenna designs (P-S).

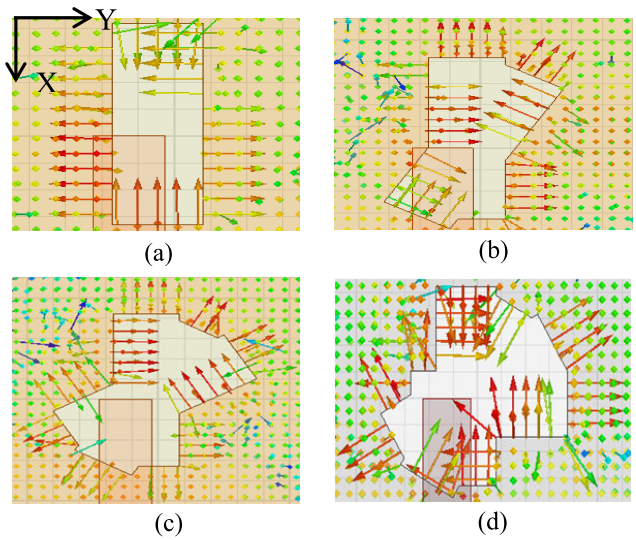

FIGURE 7. E-field distribution during different rotation of asymmetrical rectangular slots from the vertical slot to horizontal slot direction (a) Antenna 'P' at 5.28 GHz (b) Antenna 'Q' at 5.8 GHz (c) Antenna 'R' at 5.7 GHz (c) Antenna 'S' at 5.4 GHz (Proposed design).

slots. A comparison table between case-1 and case-2 has shown in TABLE-2

In this perspective, various structures (Antenna A, B and C) based on different rotation angles 'θ' of the rectangular slots have shown in Table-3 and their respective E-field distributions have also shown in Table-3. In Fig. 9(a) and Fig. 9(b), the reflection coefficient and AR variation for different antenna structures (A, B and C) have shown, respectively. From Fig. 9(a), it is noticed that if the rotation angle is increased first resonant frequency of the input reflection coefficient shifted in the lower frequency side. Therefore, the

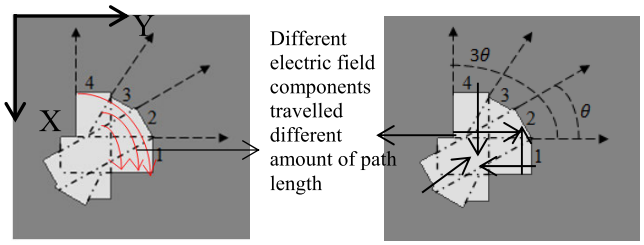

FIGURE 8. E-field distribution inside the asymmetrical bow-tie shape slot for different path length covered by electric field components.

TABLE 2. Comparison table for case-1 and case-2.

Case-1 Antenna	$\|S_{11}\|$ %	AR %	Case-2 Antenna	$\|S_{11}\|$ %	AR %
W	1.7	0	P	0	3.59, 2.15
X	4.03	0	Q	6.5, 2.86	0
Y	21.31	0	R	30.63	13.91
Z (Proposed)	27.01	27.44	S (Proposed)	27.01	27.44

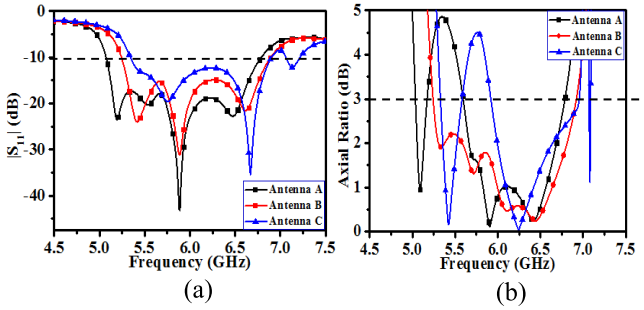

FIGURE 9. (a) $|S_{11}|$ and (b) AR of the different antenna design.

rotation angle directly affects the first resonant frequency because the presented antenna is a hybrid DRA and the first resonant frequency is generated due to the slot. In the hybrid DRA approach, the wideband features of the DRA are obtained by combining the frequency band of the two radiating elements of the antenna. Therefore, a wideband is generated due to the excitation of DR as well as radiation of the feeding network. So, the feed network has a major contribution to generating the wideband CP bandwidth; therefore, it excites the DR and also radiating its own in a predefined frequency range [5]. From Fig. 9(b), it has been noticed that the AR bandwidth is not similar to all structures shown in Table-3, even the fields have been decomposed. Due to different angular separations between the adjacent slots, the axial ratio bandwidth of all three cases is also not similar. The electric field components inside the rotated slots cover the different path lengths. This also confirms the phase difference between the orthogonal components of the E-field inside the rotated slots entirely depends on angular separation 'θ'. In Table 4 $|S_{11}|$ and

TABLE 3. Geometrical configuration of the different antenna design with respect to step angle 'θ' and E-field distribution (a) Antenna 'A' at 5.75 GHz (b) Antenna 'B' at 5.4 GHz (Proposed design) (c) Antenna 'C' at 5.2 GHz.

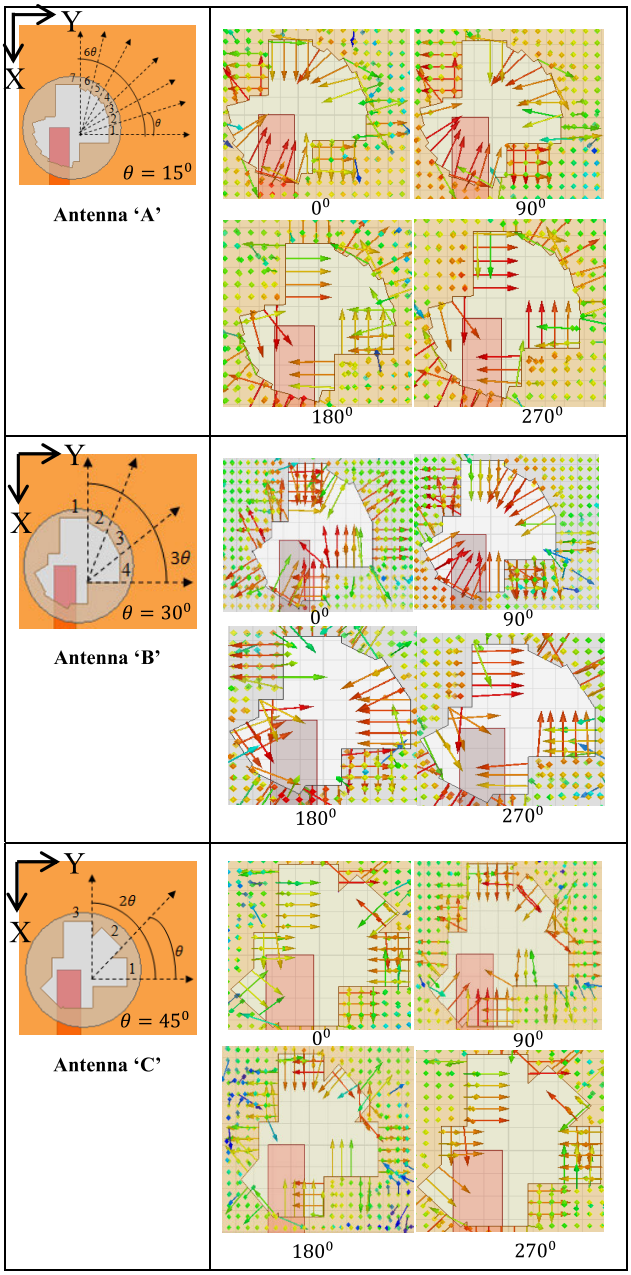

TABLE 4. $|S_{11}|$ and AR bandwidth for different antenna design (A, B & C) (shown in table 3) with respect to different step angles 'θ'.

Antenna	Impedance Bandwidth %	Axial Ratio Bandwidth %
A	28.66	(2.54 & 19.06)
B	27.01	27.44
C	(25.30 & 1.96)	(4.58 & 16)

AR results for different antenna design (A, B & C) with respect to different step angles 'θ' has shown.

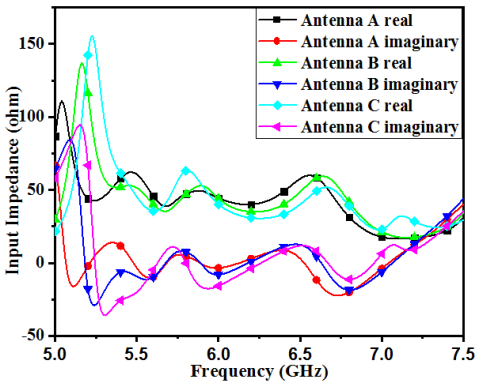

FIGURE 10. Input impedance versus frequency curve of the different antenna design.

However, for different rotation angles of the adjacent slots both the resonant peaks and matching frequency ranges are shifted with respect to their step angles. In this perspective, input impedance versus frequency curves of the different antenna designs (A, B and C) has shown in Fig. 10. Antenna-A (with 15° rotation angle), the matching frequency ranges are (5.08 - 6.78) GHz with resonant frequency at 5.19 GHz, 5.54 GHz, 5.89 GHz and 6.47 GHz. Antenna-B, (with 30° rotation angles), the matching frequency ranges are (5.25 - 6.89) GHz with the resonant frequency at 5.42 GHz, 5.89 GHz and 6.62 GHz. Antenna-C, the matching frequency ranges are from (5.35 - 6.9) GHz and (7.07 - 7.21) GHz with resonant frequency 5.75 GHz, 6.67 GHz and 7.13 GHz, respectively. This indicates that the resonant frequency is very sensitive to the rotation angle of the slot. So, it is observed that in each case the real and imaginary parts are near about 50 ohms and 0 ohm, respectively. In the case of Antenna-C, the resonant frequency is shifted more as compared to (Antenna-A and Antenna-B) and wider axial ratio bandwidth is achieved in the case of Antenna-B as compared to Antenna A and C.

B. GENERATION OF CIRCULAR POLARIZATION

In the proposed structure, two orthogonal modes of CDRA similar to $\mathbf{HE_{11\delta}}$ mode at 5.9 GHz and 6.6 GHz, respectively, are excited to achieve the wideband CP bandwidth. For introducing a 90° angular separation between the two linearly polarized E-field components, an asymmetrical bow-tie-shaped slot is embedded in the proposed design. Therefore, rotated slots are introducing gradual orthogonality between the field components. The effect of DRA on input reflection coefficient and axial ratio response with respect to frequency has shown in Fig. 11. From Fig. 11(a) it is concluded that without DRA except for the first resonant peak (5.4 GHz), the remaining two resonant peaks (at 5.9 GHz and 6.6 GHz) have vanished. Therefore, the first resonant peak is excited due to the slot and the remaining two resonant peak is coming due to CDRA.

The five design stages of the reported CP antenna have been shown in Fig. 12, to demonstrate the operating principle

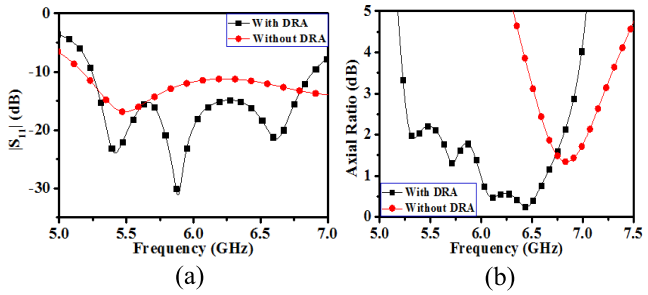

FIGURE 11. (a) $|S_{11}|$ and (b) AR of the proposed antenna with and without DRA.

of the presented CP DRA. From Fig. 12, in each step starting from step 1 to step 5, in the ground plane, rectangular slots are introduced step by step. The simulated graph of the magnitude of the E-field components (i.e. Ephi/Etheta) and angle between the Ephi and Etheta (in degree) with respect to frequency of all five stages of the proposed antenna configuration as shown in Fig. 13. To generate CP fields, these conditions must be fulfilled, the two orthogonal linear components of the field must be presented with the same magnitude and must have a phase difference of odd multiples of 90°. In stage 1, a cylindrical dielectric resonator (CDR) is excited by symmetric aperture feed i.e. the microstrip line is placed centrally with respect to the rectangular slot. But in this case, only one field component is excited, i.e. Ephi and Etheta∼0 tend to zero magnitude. Therefore, it does not fulfill the CP condition. In step 2, to introduce the Etheta component, an off-centered microstrip feed is used to excite the CDR which is shown in Fig. 12 and Fig. 13, respectively. In the third stage, i.e. step 3, rectangular slot '2' is introduced to increase the magnitude of the Etheta component, but its magnitude is not equal to the Ephi component. Due to that slot '3' is introduced in step 4, to again increase the magnitude of the Etheta component but still, its magnitude is not equal to the Ephi component over the entire AR frequency range. In step 5, rectangular slot '4' is introduced, resulting magnitude of Ephi and Etheta is almost equal over the entire AR frequency range and 90° phase difference between the E-field components are also achieved.

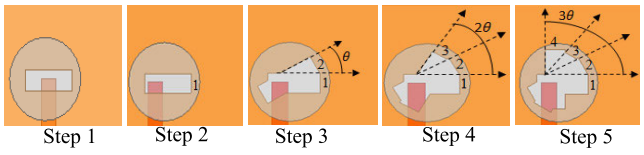

FIGURE 12. The design procedure for antenna prototypes.

C. PARAMETRIC ANALYSIS OF THE PROPOSED ANTENNA DESIGN

The $|S_{11}|$ and AR variation for different slot lengths 'd' have shown in Fig. 14(a) and 14(b). With an increase in slot length 'd', the first resonant frequency goes

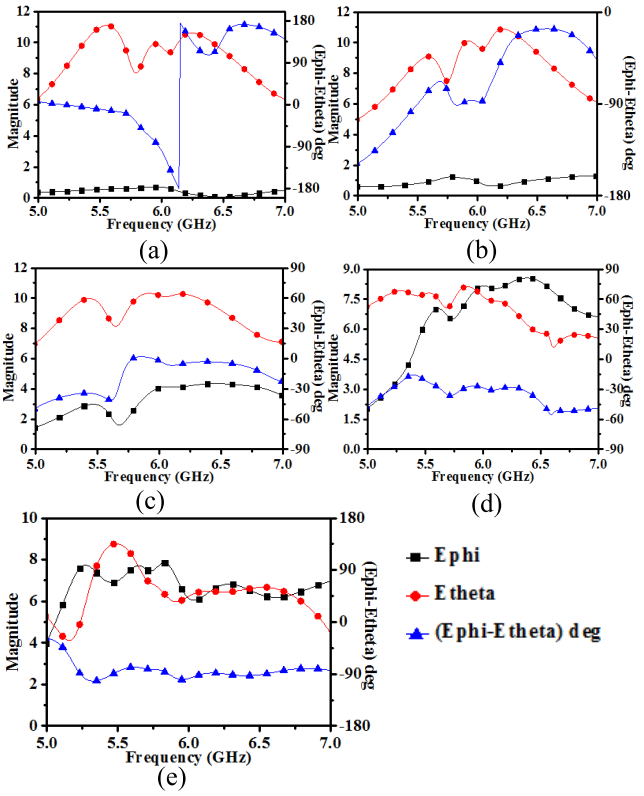

FIGURE 13. Simulated magnitude of the E-field components and angle between the E-field components (in degree) of all five stages of the proposed antenna configuration.

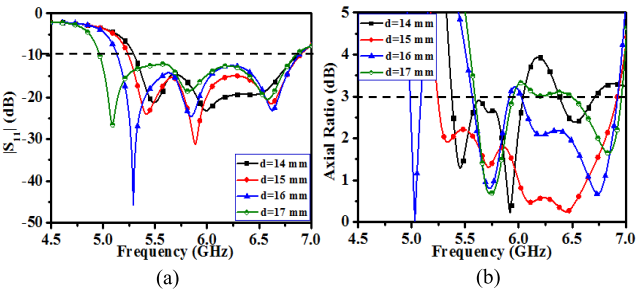

FIGURE 14. The effect of slot length 'd' variation on (a) $|S_{11}|$ (b) AR.

in the lower frequency region as compared to the second and third resonant frequencies. The presented antenna is a hybrid DRA and the first resonant frequency is generated due to the slot. Therefore, any changes in slot dimension directly affect the first resonant frequency of the reflection coefficient response. Similarly, from Fig. 14(b), the AR bandwidth also minimizes if slot length varies from 14 mm to 17 mm and it becomes lower for d = 17 mm. Therefore, to achieve maximum AR bandwidth, the slot length of d = 15 mm is fixed for the final optimized design. Table 5 illustrates the $|S_{11}|$ and CP bandwidth for different lengths of the slot (d).

In Fig. 15(a) and Fig. 15(b), the effect of different slot width 'b' on $|S_{11}|$ and CP bandwidth is similar to slot

TABLE 5. Impedance and axial ratio bandwidth for different slot length.

Slot length (d) in mm	IM BW (GHz & %)	AR BW (GHz & %)
14	(5.3 – 6.87), 25.8	(5.38 – 6.04), 11.55 (6.38 – 6.71), 5.04
15	(5.25 – 6.89), 27.01	(5.25 – 6.92), 27.44
16	(5.14 – 6.88), 28.95	(4.99 – 5.08), 1.78 (5.57 – 5.91), 5.92 (6.03 – 6.92), 13.74
17	(4.97 – 6.85), 31.81	(5.6 – 5.94), 5.89 (6.5 – 6.96), 6.83

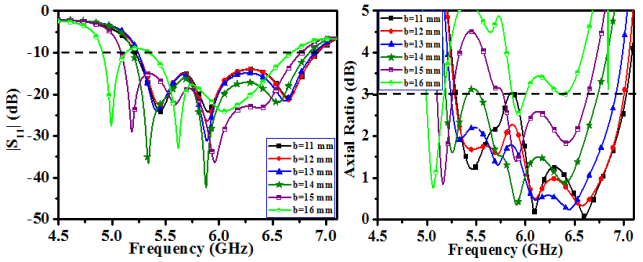

FIGURE 15. The effect of slot length 'b' variation on (a) $|S_{11}|$ (b) AR.

length 'd' has shown. It is found that the greater CP bandwidth is produced for the case b = 13 mm.

Fig. 16 explains the effect of the displacement (D) of the microstrip line along the y-axis direction. As 'D' increases from 14.5 mm to 17.5 mm, it affects the impedance matching of the reflection coefficient and also reduces the impedance bandwidth. In the case of AR, if 'D' increases or decreases, it is reduced to a lower value for both conditions. The maximum impedance and CP bandwidth have been produced for the case D = 15.5 mm.

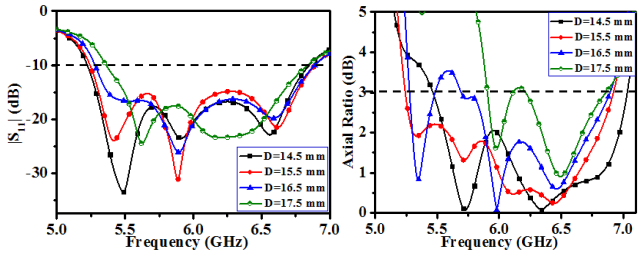

FIGURE 16. Displacement of Microstrip line position 'D' with respect to the center of the substrate in the y-direction (a) $|S_{11}|$ (b) AR.

IV. EXPERIMENTAL RESULTS

Based on optimized parameters proposed in Fig. 1, a prototype of the presented CP design has been fabricated to verify the HFSS results. In Fig. 17, a clear picture of the fabricated DRA has been displayed. The measurement of the input reflection coefficient of the fabricated DRA has been displayed. The measurement of the input reflection

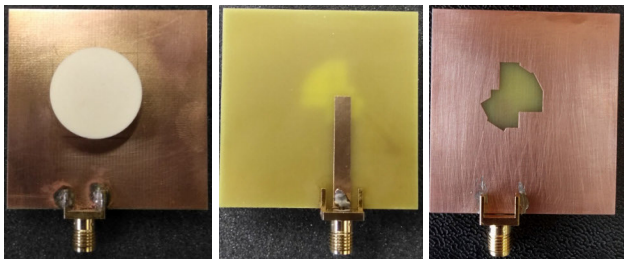

FIGURE 17. Fabricated antenna photographs (a) Top view (b) Microstrip feeding (c) Slot geometry.

coefficient of the fabricated DRA has been done through the Keysight Performance Network Analyzer (PNA) N5221A (10 MHz - 13.5 GHz). Fig. 18(a) illustrates that the input reflection coefficient ($|S_{11}| < -10$ dB) response as a function of frequency. From Fig. 18(a), the simulated and experimental impedance bandwidth of 27.01% and 26.73% is achieved by the presented structure, respectively. The reflection coefficient response shows that the novel agreement between the experimental and simulated curve. Some minor discrepancies occurred between the experimental and simulated outcomes which may be generated due to fabrication errors.

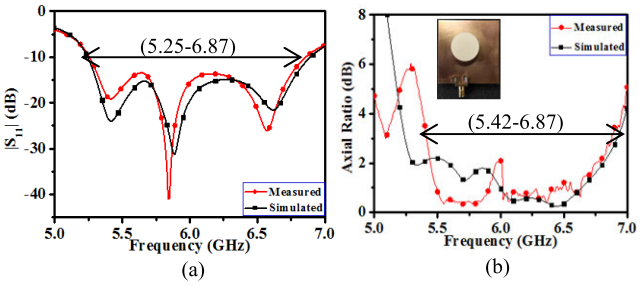

FIGURE 18. Simulated and experimental results (a) $|S_{11}|$ (b) AR.

A. AXIAL RATIO

The far-field parameters have been measured along the boresight direction, i.e. ($\theta = 0$ and $\phi = 0$). Fig. 18(b) illustrates the simulated and experimental CP bandwidth of 27.44% and 23.59%, respectively. A slight difference is observed between the measured and simulated AR result which may be also created due to fabrication tolerances such as the use of adhesive material for placing the DR onto the slot which is not considered at the time of simulation or a slight displacement of DR from its exact position. Table 6 illustrates the AR performance of the presented CP antenna according to the operating frequency ranges and % bandwidth.

B. RADIATION PATTERNS

For two planes, i.e. ($\phi = 0°$ and $\phi = 90°$), the proposed structure radiation pattern has been experimentally tested. Fig. 19 and Fig. 20 explain the simulated and experimental radiation pattern at 5.7 GHz and 6.4 GHz respectively,

TABLE 6. Performance of the proposed antenna.

Parameters	-10-dB Impedance Bandwidth		3-dB Axial Ratio Bandwidth	
	Simulated	Measured	Simulated	Measured
Operating Frequency Range in GHz	(5.25-6.89)	(5.25–6.87)	(5.25-6.92)	(5.42–6.87)
% Bandwidth	27.01 %	26.73 %	27.44 %	23.59 %

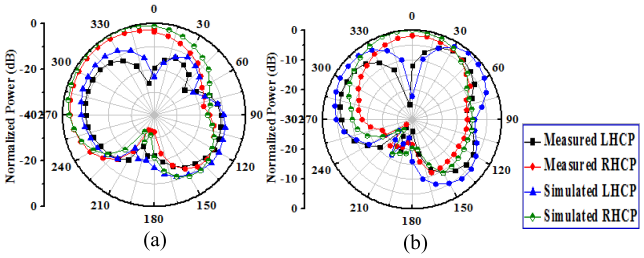

FIGURE 19. LHCP/RHCP pattern at 5.7 GHz on (a) XZ plane (b) YZ plane.

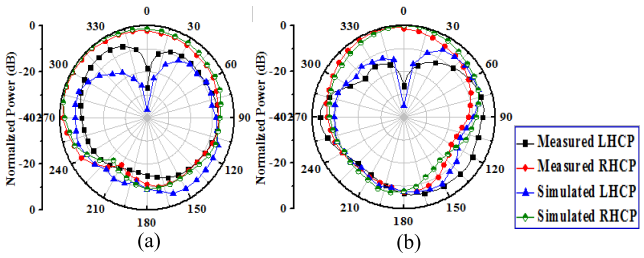

FIGURE 20. LHCP/RHCP pattern at 6.4 GHz on (a) XZ plane (b) YZ plane.

for two principle planes, i.e. (*xz* and *yz*) of the proposed antenna. From Fig. 19, at 5.7 GHz, the component of the right-hand CP (RHCP) field is greater than the left-hand CP (LHCP) field by 30 dB and 20 dB along the broadside direction in two principles (*xz*- and *yz*-) planes, respectively. Fig. 20 also illustrates that the proposed antenna radiation pattern at 6.4 GHz and the observation shows that the RHCP field is also greater than the LHCP field by 20 dB and 30 dB for both planes such as (*xz* and *yz*), respectively. Fig. 19(a) and 19(b) the beamwidth at 5.7 GHz is (82°) and (60°), respectively. Fig. 20(a) and 20(b), the 3-dB beamwidth at 6.4 GHz is (128°) and (78°), respectively.

C. SENSE OF POLARIZATION

The direction of rotation of the rectangular slot decides the sense of antenna polarization. Circular polarization can be generated by properly selecting the rotation angle of the rectangular slot. Here, each slot is rotated by 30° with respect to its contiguous slots, therefore the total angular separation of 90° is created by the four rotated rectangular slots. The RHCP and LHCP conversion mechanism is shown in Fig. 21.

TABLE 7. CP performance of the presented antenna in comparison with other cp draS reported earlier in the literature.

DRA Shape	Feeding	ε_r	f_{cp} (GHz)	S_{11} (% & GHz)	BW_{CP} (% & GHz)	Gain (dBi)
Cylindrical DRA [21]	Annular slot with opposing stubs	9.5	1.96	18	3.4	4.5
Cylindrical DRA [22]	Circular shaped aperture	9.8	2.6/5.15	18.04 & (2.42-2.90)/ 19.85 & (4.9-5.68)	6.45 & (2.55-2.72)/ 14.74 & (4.9-5.68)	5.5/6
Four Rectangular Dielectric Layers [17]	Aperture coupling	10.2	9.5	21 & (8.9-11)	6 & (9.55-10.15)	6-6.7
Bow-tie shaped [6]	Asymmetric cross-slot	10.2	8.1	43.8 & (6.5-10.75)	7.4 & (7.8 – 8.4)	5.8
Cylindrical [This work]	Asymmetrical bow-tie shaped slot	9.8	5.5/6/6.5	26.73 & (5.25-6.87)	23.59 & (5.42-6.87)	3.4

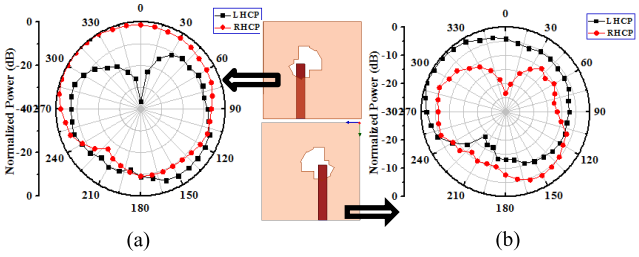

FIGURE 21. Simulated radiation pattern at 6.4 GHz on XZ-plane (a) For RHCP operation (b) For LHCP operation.

According to Fig. 21(a) slot position, the RHCP field will be generated, and by taking a mirror image of Fig. 21(a), the RHCP field is converted into the LHCP field which has shown in Fig. 21(b).

D. GAIN AND RADIATION EFFICIENCY

The experimental and simulated gain curve variation with respect to frequency has explained in Fig. 22 and the maximum measured gain of 3.4 dB is delivered by the presented CP antenna. Hybrid DRA is the combining effect of the

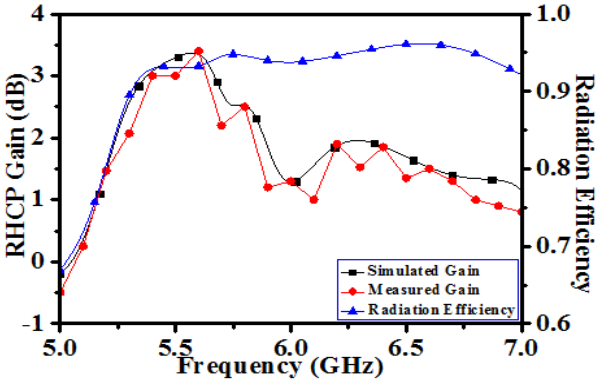

FIGURE 22. Simulated and measured RHCP gain and radiation efficiency response of the presented CP antenna at ($\theta = 0°$ & $\phi = 0°$).

dielectric resonator and some other radiating element in the antenna structure [18], [19]. This method provides the advantage of compactness along with independent control over the different frequency bands. But, it suffers from high fluctuation in gain value over the operating frequency bands [20]. Fig. 22 also discussed the radiation efficiency of the presented CP DRA with respect to frequency and the radiation efficiency of 95% has also obtained over the frequency range 5 to 7 GHz. A comparison table of the proposed antenna with other slot-fed DRAs has shown in TABLE 7 and the proposed CP DRA shows better CP performance as compare to the listed CP DRAs in the below table.

V. CONCLUSION

In this paper, a circularly polarized slot-coupled cylindrical DRA excited by an off-centered microstrip line has been investigated for WLAN application. The proposed configuration is achieved the measured impedance and CP bandwidth of 26.73% and 23.59%, respectively. The entire AR bandwidth is covered the impedance frequency range and the complete AR frequency range is usable. The mirror image of the presented CP design is switched the RHCP field into the LHCP field. The maximum RHCP gain of 3.4 dB has been achieved by the designed antenna.

REFERENCES

[1] A. Petosa, *Dielectric Resonator Antenna Handbook*. Norwood, MA, USA: Artech House, 2007.
[2] A. Perron, T. A. Denidni, and A. R. Sebak, "Circularly polarized microstrip/elliptical dielectric ring resonator antenna for millimeter-wave applications," *IEEE Antennas Wireless Propag. Lett.*, vol. 9, pp. 783–786, 2010.
[3] Y. M. Pan, K. W. Leung, and K. Lu, "Omnidirectional linearly and circularly polarized rectangular dielectric resonator antennas," *IEEE Trans. Antennas Propag.*, vol. 60, no. 2, pp. 751–759, Feb. 2012.
[4] K.-W. Khoo, Y.-X. Guo, and L. C. Ong, "Wideband circularly polarized dielectric resonator antenna," *IEEE Trans. Antennas Propag.*, vol. 55, no. 7, pp. 1929–1932, Jul. 2007.
[5] G. Massie, M. Caillet, M. Clenet, and Y. M. M. Antar, "A new wideband circularly polarized hybrid dielectric resonator antenna," *IEEE Antennas Wireless Propag. Lett.*, vol. 9, pp. 347–350, 2010.
[6] P. Chauthaiwale, R. K. Chaudhary, and K. V. Srivastava, "Circularly polarized bowtie-shaped dielectric resonator antenna excited with asymmetric cross slot," *Microw. Opt. Technol. Lett.*, vol. 57, no. 7, pp. 1723–1727, Jul. 2015.
[7] W. C. Wong and K. W. Leung, "Circularly polarized dielectric resonator antenna excited by dual conformal strips of unequal lengths," *Microw. Opt. Technol. Lett.*, vol. 29, no. 5, pp. 348–350, 2001.
[8] Y. Pan, K. W. Leung, and E. H. Lim, "Compact wideband circularly polarized rectangular dielectric resonator antenna with dual underlaid hybrid couplers," *Microw. Opt. Technol. Lett.*, vol. 52, no. 12, pp. 2789–2791, Dec. 2010.
[9] E. H. Lim, K. W. Leung, and X. S. Fang, "The compact circularly-polarized hollow rectangular dielectric resonator antenna with an underlaid quadrature coupler," *IEEE Trans. Antennas Propag.*, vol. 59, no. 1, pp. 288–293, Jan. 2011.
[10] K. K. Pang, H. Y. Lo, K. W. Leung, K. M. Luk, and E. K. N. Yung, "Circularly polarized dielectric resonator antenna subarrays," *Microw. Opt. Technol. Lett.*, vol. 27, no. 6, pp. 377–379, 2000.
[11] S.-L.-S. Yang, R. Chair, A. A. Kishk, K.-F. Lee, and K.-M. Luk, "Study on sequential feeding networks for subarrays of circularly polarized elliptical dielectric resonator antenna," *IEEE Trans. Antennas Propag.*, vol. 55, no. 2, pp. 321–333, Feb. 2007.
[12] M. Yang, Y. Pan, and W. Yang, "A singly fed wideband circularly polarized dielectric resonator antenna," *IEEE Antennas Wireless Propag. Lett.*, vol. 17, no. 8, pp. 1515–1518, Aug. 2018, doi: 10.1109/LAWP.2018.2851574.
[13] S. Liu, D. Yang, Y. Chen, S. Huang, and Y. Xiang, "Broadband dual circularly polarized dielectric resonator antenna for ambient electromagnetic energy harvesting," *IEEE Trans. Antennas Propag.*, vol. 68, no. 6, pp. 4961–4966, Jun. 2020, doi: 10.1109/TAP.2020.2968768.
[14] W.-J. Sun, W.-W. Yang, P. Chu, and J.-X. Chen, "Design of a wideband circularly polarized stacked dielectric resonator antenna," *IEEE Trans. Antennas Propag.*, vol. 67, no. 1, pp. 591–595, Jan. 2019, doi: 10.1109/TAP.2018.2874678.
[15] M.-D. Yang, Y.-M. Pan, Y.-X. Sun, and K.-W. Leung, "Wideband circularly polarized substrate-integrated embedded dielectric resonator antenna for millimeter-wave applications," *IEEE Trans. Antennas Propag.*, vol. 68, no. 2, pp. 1145–1150, Feb. 2020, doi: 10.1109/TAP.2019.2938629.
[16] R. Chowdhury and R. K. Chaudhary, "An approach to generate circular polarization in a modified cylindrical-shaped dielectric resonator antenna using PMC boundary approximation," *IEEE Antennas Wireless Propag. Lett.*, vol. 17, no. 9, pp. 1727–1731, Sep. 2018.
[17] S. Fakhte, H. Oraizi, and R. Karimian, "A novel low-cost circularly polarized rotated stacked dielectric resonator antenna," *IEEE Antennas Wireless Propag. Lett.*, vol. 13, pp. 722–725, 2014.
[18] Y. Ding, K. W. Leung, and K. M. Luk, "Compact circularly polarized dualband zonal-slot/DRA hybrid antenna without external ground plane," *IEEE Trans. Antennas Propag.*, vol. 59, no. 6, pp. 2404–2409, Jun. 2011.
[19] A. Sharma and R. K. Gangwar, "Compact dual-band ring dielectric resonator antenna with moon-shaped defected ground structure for WiMAX/WLAN applications," *Int. J. RF Microw. Comput.-Aided Eng.*, vol. 26, no. 6, pp. 503–511, Aug. 2016.
[20] P. Gupta, D. Guha, and C. Kumar, "Dielectric resonator working as feed as well as antenna: New concept for dual-mode dual-band improved design," *IEEE Trans. Antennas Propag.*, vol. 64, no. 4, pp. 1497–1502, Apr. 2016.
[21] K. W. Leung and S. K. Mok, "Circularly polarised dielectric resonator antenna excited by perturbed annular slot with backing cavity," *Electron. Lett.*, vol. 37, pp. 934–936, Aug. 2001.
[22] A. Sharma, G. Das, and R. K. Gangwar, "Dual-band circularly polarized modified circular aperture loaded cylindrical dielectric resonator antenna for wireless applications," *Microw. Opt. Technol. Lett.*, vol. 59, no. 7, pp. 1562–1570, Jul. 2017.

REENA KUMARI received the Bachelor of Engineering degree in electronics and communication engineering from the Birla Institute of Technology, Ranchi, Jharkhand, India, in 2010, and the Ph.D. degree in electronics engineering from IIT (Indian School of Mines) Dhanbad, in 2019. She is currently an Assistant Professor with the Department of Electronics and Communication Engineering, Vignan's Foundation For Science, Technology and Research (VFSTR), Vadlamudi, Andhra Pradesh, India. She has authored over 12 research articles in international journal/conference proceedings. Her research interest includes circularly polarized dielectric resonator antennas. She has also served as a Reviewer for IEEE Antennas and Wireless Propagation Letters and the *International Journal of RF and Microwave Computer-Aided Engineering*.

RAVI KUMAR GANGWAR (Senior Member, IEEE) received the B.Tech. degree in electronics and communication engineering from Uttar Pradesh Technical University, Lucknow, and the Ph.D. degree in electronics engineering from the Indian Institute of Technology (Banaras Hindu University) at Varanasi, Varanasi, India, in 2006 and 2011, respectively.

He is currently an Associate Professor with the Department of Electronics Engineering and an Associate Dean (Sponsored Research and Industrial Consultancy) of the Indian Institute of Technology (Indian School of Mines) Dhanbad, India. He is guided/guiding 15 Ph.D. and 19 M.Tech. students. He has completed/ongoing eight research and development projects (≈2 Crores rupees) related dielectric resonator antennas and their applications from various funding agencies, like DRDO, SERB-DST, and ISRO. He has authored or coauthored over 100 research articles in reputed international journals and 80 papers in conference proceedings. His research interests include dielectric resonator antennas, microstrip antennas, and bio-electromagnetics.

Dr. Gangwar is a Senior Member of the Antenna and Propagation Society, the Institute of Electrical and Electronics Engineers (IEEE), USA, a member of the Institution of Engineering and Technology (IET), U.K., a Life Member of the Institution of Engineers (IE), India, and a fellow of the Institution of Electronics and Telecommunication Engineers (IETE), India. He is also a member of the IETE Executive Council and a Joint Regional Secretary at the Ranchi Centre. He is an External Expert of the peer review committee of project related to chaff application of the Defence Laboratory Jodhpur, DRDO. He was a recipient of the INSA Visiting Scientist Fellowship and the IETE Smt. Ranjana Paul Memorial Award, for the year 2020. He is an Associate Editor of IEEE Access and *IET Circuits Devices and Systems* journal. He is a reviewer of IEEE Transactions of Antenna and Propagation, IEEE Antenna and Propagation Letters, *IEEE Antenna and Propagation Magazine*, *IET Microwave and Antenna Propagation*, *IET Electronics Letters*, *Microwave and Optical Technology Letters*, and *Scientific Report*.

RAGHVENDRA KUMAR CHAUDHARY (Senior Member, IEEE) received the B.Tech. degree from UIET Kanpur, India, in 2007, the M.Tech. degree from IIT (BHU) Varanasi, India, in 2009, and the Ph.D. degree from IIT Kanpur, India, in 2014. He is currently an Assistant Professor with the Department of Electronics Engineering, Indian Institute of Technology (ISM), Dhanbad, India. He has researched in developing the metamaterial antenna and dielectric resonator antennas (DRA). Development of the circularly polarized compact antenna is one of his major areas of contribution. He has guided four Ph.D. students and 15 Ph.D. students are working under him. He has published over 100 articles in top SCI journals. He was a recipient of the Young Engineers Award from the Indian National Academy of Engineering (INAE), in 2020, the Young Scientist Award from the Institution of Electronics and Telecommunication Engineers (IETE), in 2020, the Young Engineers Award from the Institution of Engineers (IEI), India, from 2019 to 2020, and many Best Paper awards in different categories in national and international conferences, such as IEEE APACE Malaysia, PIERS Singapore, and ATMS India. He has served as the Chair for the IEEE Student Branch of the Uttar Pradesh Section, for the period 2012–2013, and serving as the Counselor of the IEEE Student Branch of IIT (ISM). He is serving as an Associate Editor of *IET Microwave Antennas & Propagation*, IEEE Access, and Microwave and *Optical Technology Letters* (Wiley). He has also been featured interviewed by *Electronics Letters* (IET).